Textile Science & Research Journal
ISSN: 3059-846X Volume – 1, Issue – 1, 2025
DOI: https://doi.org/10.63456/tsrj-1-1-29

DESIGN AND PROPERTIES OF WOOL SEAMLESS GARMENT FOR OUTDOOR SPORTS BASED ON ERGONOMICS

AILAN WAN*, LILI XU, YANFEI TENG, PIBO MA

Engineering Research Center of Knitting Technology, Ministry of Education, College of Textile Science and Engineering, Jiangnan University, China

AILAN WAN: ailan.wan@jiangnan.edu.cn

Corresponding Author: AILAN WAN

ABSTRACT

To address the limitations of traditional outdoor sportswear in meeting the diverse and dynamic thermoregulatory and moisture management demands of different body regions during exercise, eight bionic knitted fabrics inspired by Victoria amazonica were prepared with wool and deodorizing spandex/polypropylene covered yarn as materials. The deodorizing, thermal-moisture comfort, and mechanical properties of the fabrics were measured. Then wool seamless garment based on ergonomics was designed resulting from comprehensive evaluation with the eight fabrics by the grey near optimal method. Also, infrared thermal imaging temperature measurement and sensory evaluation of wool seamless garment were carried out. The results showed that the main vein structure fabric had the best comprehensive performance, with air permeability rate of 390.78 mm/s and a moisture permeability rate of 454.77 g/ (m2×h). After exercise, the maximum temperature difference between the start of exercise and the third minute after exercise of the wool seamless garments for outdoor sports was 2.9℃, which was lower than the 4.4℃ difference observed in regular sportswear; the odor intensity was rated as slight, confirming its superior deodorizing properties and thermal-moisture comfort.

KEYWORDS: wool seamless garment, ergonomic design, outdoor sports, deodorizing properties, thermal-moisture comfort

INTRODUCTION

Outdoor fabrics face diverse challenges ranging from extreme cold to intense heat and form high humidity to extreme aridity. In addition, the intensity of activity and thermoregulatory demanded in different parts of the human body varied greatly during outdoor exercise. For example, wear-resistant and breathable fabrics were required for the parts of the shoulders, underarms and waists, and good freedom of movement and rapid sweating for the armpits, forechest and elbow joints.1 These complex and changeable requirements were often difficult to be satisfied by traditional integrated designs.2

Ergonomic zoned design provides an effective approach to addressing the issue of insufficient functional adaptability in traditional clothing, and recent studies have covered multiple fields: in order to adapt to diverse athletic scenarios, sportswear used the fabrics with good air permeability and moisture permeability in areas such as the chest and mid-back by the partition design.3, 4 Workwear strategically employed abrasion-resistant and thermally insulating materials in critical areas to accommodate various occupational environments.5, 6 Intelligent clothing partition systems utilized zonal differentiation to enhance recognition accuracy and optimize detection algorithms.7, 8 Smart wearable devices utilized the graded fitting of clothing in different body regions to addresses the shortcomings of traditional clothing in terms of fit and rigidity.9 Ergonomic design accommodated dynamic bodily movements providing protection and support for healthcare professionals.10, 11 However, existing studies predominantly focus on thermal-wet comfort and protective performance,12-14 while the deep integration of functionality and materials requires further strengthening. Concurrently, bio-inspired design has emerged as a significant direction for innovating functional textiles. Biological features such as the water-harvesting structure of the Namib desert beetle, the drag-reducing surface of shark skin, and the leaf venation / cavity / stomata system of the Victoria water lily have inspired advanced material development.15, 16 However, there is limited research on the odor-resistant properties of bio-inspired fabrics and the correlation between yarn materials (especially anti-odor yarns) and functionality.

Textile Science & Research Journal
ISSN: 3059-846X Volume – 1, Issue – 1, 2025
DOI: https://doi.org/10.63456/tsrj-1-1-29

This work prepared eight bionic knitted fabrics based on the Victoria amazonica with wool as the face yarn and deodorizing spandex/polypropylene covered yarn as the ground yarn. The odor resistance property, thermal-moisture comfort, and mechanical properties of the eight fabrics were tested. The grey near-optimal method was synthetically evaluated the ergonomic outdoor functional garment. The properties of the wool seamless garment based on ergonomics was ultimately assessed through infrared thermal imaging temperature measurement and sensory evaluation.

EXPERIMENTAL DETAILS

MATERIALS

2.22 tex spandex/5.56 tex72F polypropylene covered yarn with 500 twist/m were chosen as ground yarn supplied from LDZ New Aoshen Spandex Co., Ltd., China. The stretch ratio of spandex was 3.8. 11.44 tex with 70% wool and 30% polyamide was face yarn with 880 twist/m supplied from Zhejiang Xinao Textile Co., Ltd., China.

BIONIC DESIGN AND KNITTING OF WOOL FABRICS

DESIGN OF BIONIC KNITTED STRUCTURE

A promising avenue for developing advanced functional materials lies in biomimetics. The surfaces of many organisms in nature are not smooth but are composed of functionally unique structures honed by natural evolution to survive in harsh environments.17, 18 A notable example is Victoria amazonica, which possesses distinctive microstructures on both its petioles and leaf surfaces. These structures, including its venation network and cavity systems, have found extensive applications in biomimetic research, inspiring designs for buoyancy, strength, and fluid transport.19-21 As shown in Figure 1, the leaf and vein morphology revealed primary and secondary branch structures. The main vein was relatively thick and radially diffused, and the secondary vein connected the main vein to form small grids of random dislocation arrangement. Both cross-sectional and longitudinal sections contained numerous air-filled pores resembling gas passages, which facilitated temperature regulation and water transport. Simultaneously, the vein distribution created bubble-like protrusions on the leaf's upper surface. The surface was also densely distributed with many small pores of help to exude the accumulated rainwater on the leaf surface, assist respiration, and prevented leaf decay.

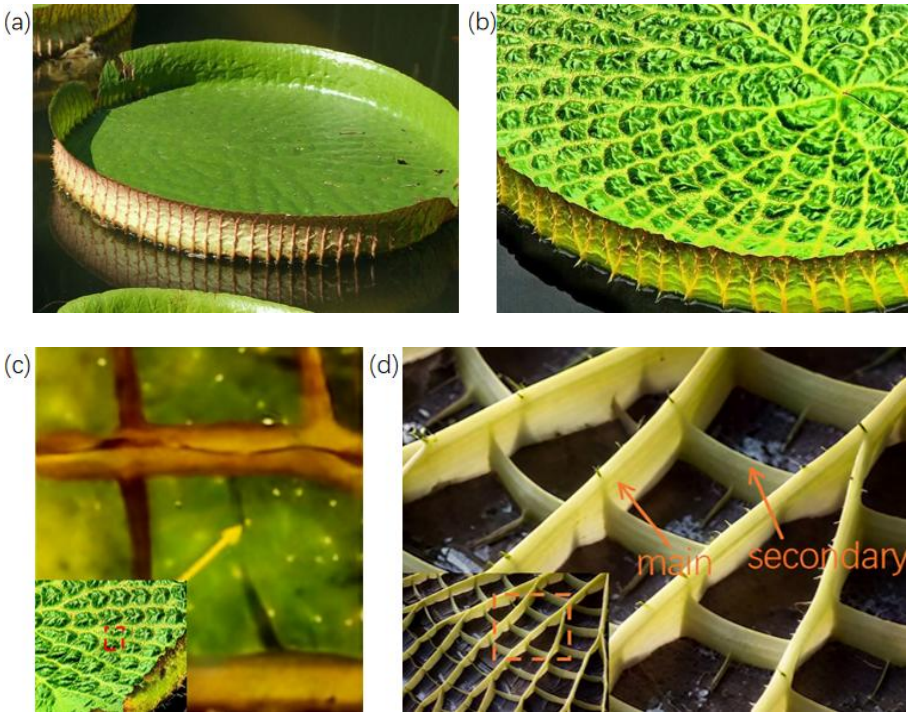

Textile Science & Research Journal
ISSN: 3059-846X Volume – 1, Issue – 1, 2025
DOI: https://doi.org/10.63456/tsrj-1-1-29

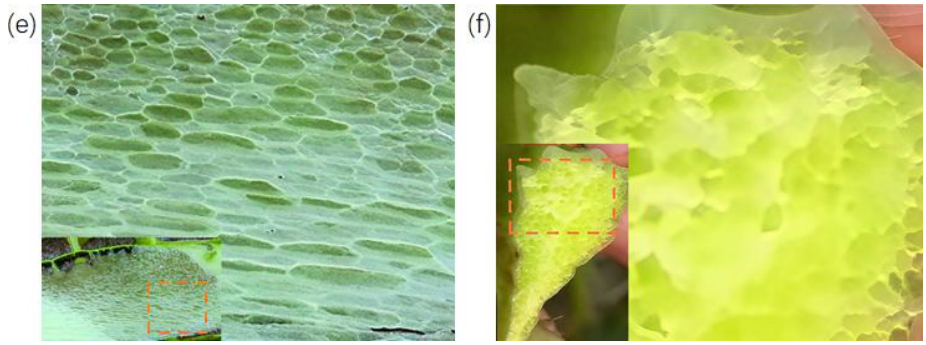

Figure 1. Pictures of Victoria amazonica22. (a) The Victoria amazonica; (b) Leaf of the Victoria amazonica; (c) Small holes (yellow arrow) on the leaves; (d) Underside of the leaf showing veins network; (e) Longitudinal-section and cavities of leaf veins; (f) Cross-section of the leaf vein

Eight bionic knitted fabrics were inspired by the venation arrangement, cavity structure, and stomatal structure of the leaves. Tissue diagrams (PAT) were drawn in the graphic design software (Photon). The knitting state of a coil on the fabric was represented by colored squares (yellow, black, and red). A yellow square indicated that the ground yarn and the face yarn formed loops on the needles simultaneously, creating a weft-knitted plain structure. A black square indicated that the selection needle system did not feed yarn, and both the face yarn and the ground yarn floated on the back of the fabric. So the fabric contracted in the Y and Z directions under the action of yarn tension, creating a wrinkled effect similar to the leaf vein pore channels, as shown in Figure 2(a). A red square indicated that the ground yarn formed a loop on the needle while the face yarn did not. In this case, the face yarn floated on the back of the fabric and created micro-pores that functionally mimicked leaf stomata, as shown in Figure 2(b).

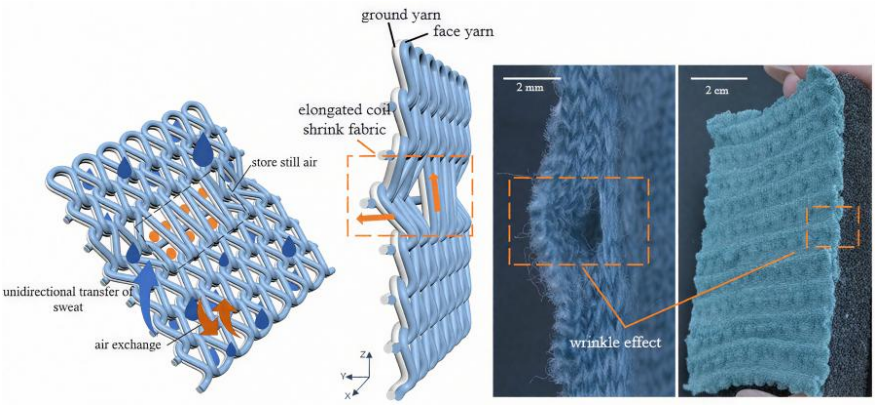

(a) Stitch knitting model of black grid

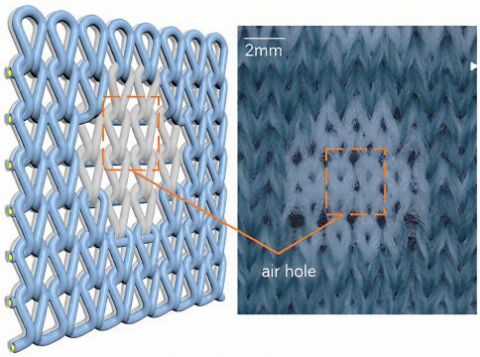

(b) Stitch knitting model of red grid

Figure 2. Stitch pattern diagram. (a) Stitch knitting model of black grid; (b) Stitch knitting model of red grid

Textile Science & Research Journal
ISSN: 3059-846X Volume – 1, Issue – 1, 2025
DOI: https://doi.org/10.63456/tsrj-1-1-29

As illustrated in Figure 3, the eight biomimetic structural pattern designs were derived from the venation arrangement and morphological characteristics of Victoria amazonica leaves, achieved through controlled spatial distribution and quantitative variations of the yellow, black, and red square elements.

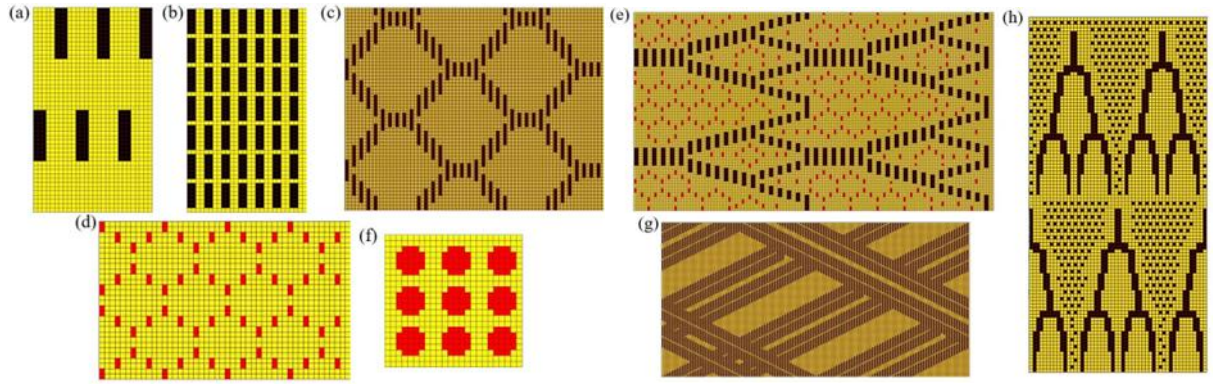

Figure 3. Bionic vein structure fabric PAT diagram. (a)Main vein; (b)Secondary vein; (c)Vein small grid; (d)Leaf small pore; (e)Branching structure I; (f)Leaf big pore; (g)Bubble structure; (h) Branching structure II

KNITTING OF FABRIC

All the fabrics were knitted on a seamless knitting machine (SM8-TOP2 MP2, Santoni, Italy) in Figure 4. The machine had a gauge of 28, a cylinder diameter of 15 inches, 1344 needles, 8 yarn feeders, a feed tension of 2.5 cN, and a density control position of 11. The specifications of fabrics were listed in Table 1.

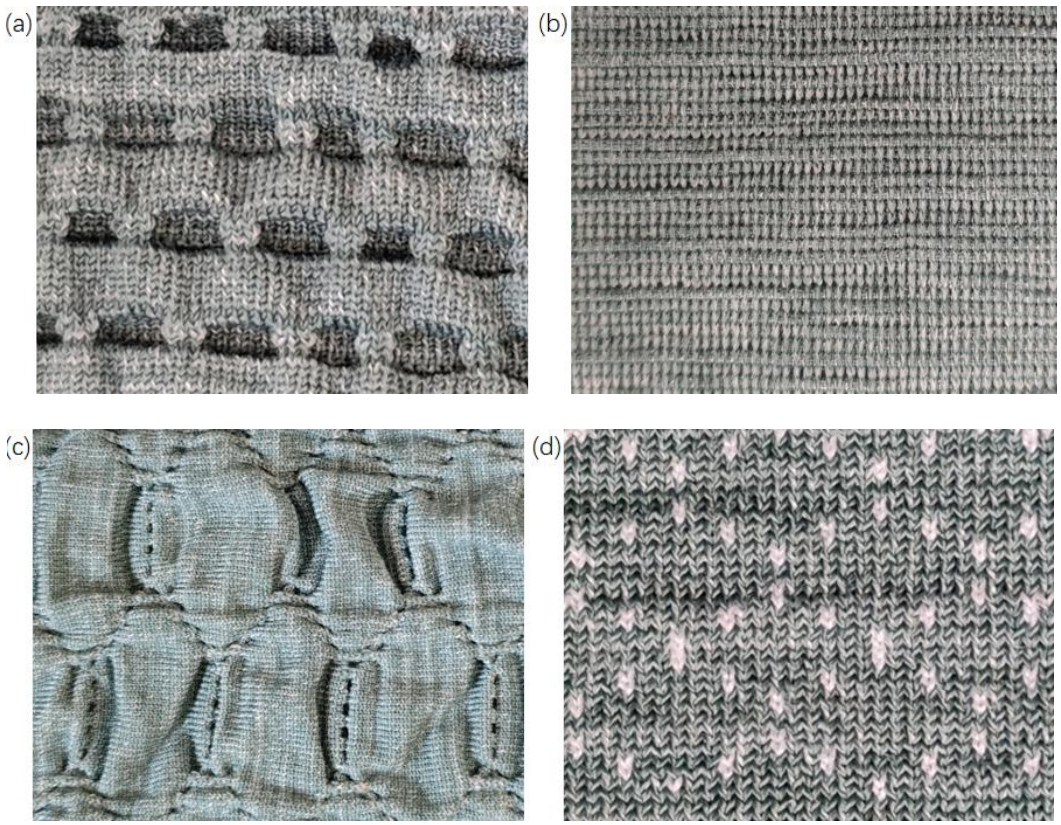

Textile Science & Research Journal
ISSN: 3059-846X Volume – 1, Issue – 1, 2025
DOI: https://doi.org/10.63456/tsrj-1-1-29

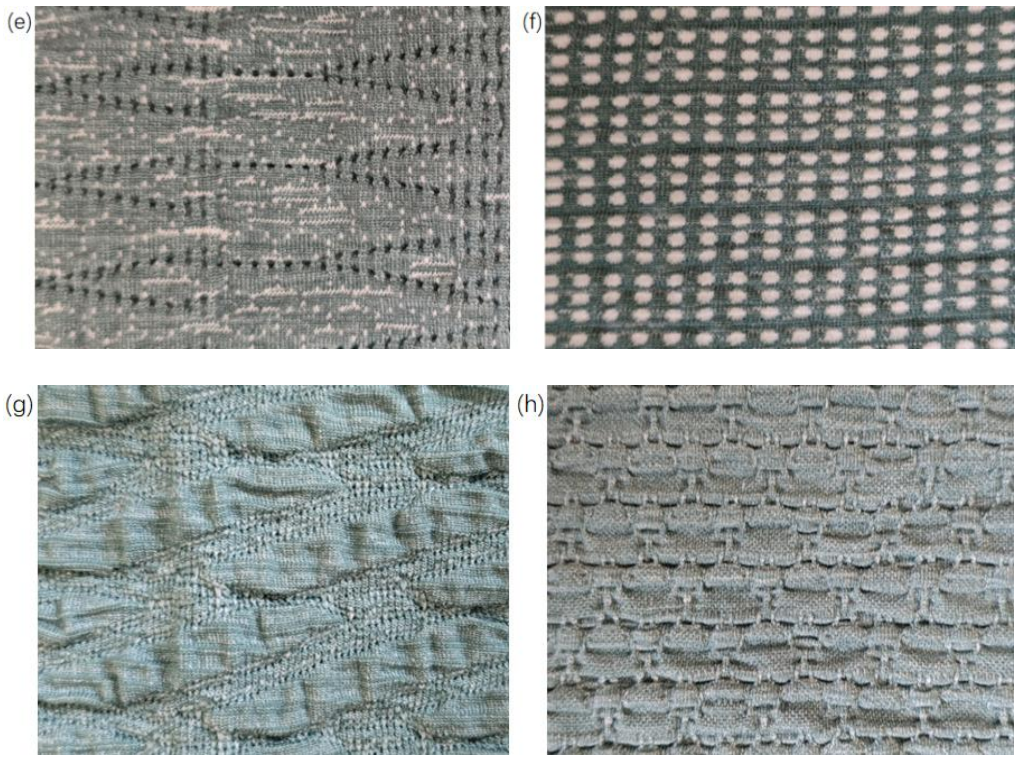

Figure 4. Knitted stitches photos of imitating vein structure, (a) and (b) the pore architecture of the Victoria amazonica leaf veins, (c) combining the main veins and secondary veins, (d) and (f) the microscopic stomatal structures on the leaf surface, (e) the horizontal arrangement of the vein branch structure, added small concave air holes to imitate the entire leaf shape, , (g) the bubble-like shape of the leaf surface, (h) the longitudinally arranged recessed holes of a branching structure.

Table 1. Specifications and structure parameters of fabrics

Structure	Sample NO.	Areal density ($g \times m^{-2}$)	Thickness (mm)	Density (Number of loops×$(5cm)^{-1}$)		DPUF content	Wool content
				Horizontal	Vertical		
Main vein	1#	339	2.28(0.15)	95	165	12.93%	60.64%
Secondary vein	2#	326	1.44(0.08)	100	245	12.81%	60.54%
Vein small grid	3#	340	2.23(0.13)	75	185	11.65%	64.50%
Leaf small pore	4#	218	0.83(0.03)	80	145	13.59%	58.39%
Branching structure I	5#	252	1.50(0.05)	70	165	12.97%	60.29%
Leaf big pore	6#	199	0.96(0.06)	80	145	14.85%	54.60%
Bubble structure	7#	442	2.17(0.11)	90	220	12.70%	61.19%
Branching structure II	8#	331	1.89(0.10)	85	195	12.78%	60.85%
Weft jersey	0#	310	1.06(0.07)	95	155	12.37%	62.14%

DPUF: deodorant spandex

Textile Science & Research Journal
ISSN: 3059-846X Volume – 1, Issue – 1, 2025
DOI: https://doi.org/10.63456/tsrj-1-1-29

ERGONOMIC DESIGN AND KNITTING OF WOOL SEAMLESS GARMENTS

DESIGN OF THE SEAMLESS GARMENT BASED ON ERGONOMICS

During outdoor activities, the human body rapidly generates significant heat accumulation and perspiration due to muscular activity and activated sweat glands. To address these challenges, a precision functional partitioning design was developed with thermophysiological responses by outdoor athletic activities.

Thermal distribution during high-intensity activity shouws significant regional variation. Adipose tissue was concentrated around the organs in the chest and abdominal cavities, the muscle groups were mainly distributed in the chest, abdomen, and limbs, while the proportion of muscle groups in the back was relatively small. During exercise, the organs and muscles located on both sides of the chest and abdomen were very active, the blood circulation was fast, and the heat generated was the most. The arms also generated a significant amount of heat through the movement of muscle groups. In contrast, the chest, back, and waist produced relatively less heat.

Moisture distribution across the human body during high-intensity exercise is primarily regulated by sweat glands, which are distributed throughout the body and essential for thermoregulation and physiological homeostasis. Sweat glands are categorized into two types: eccrine glands, predominantly localized in regions such as the axillae, chest, and dorsal torso, and apocrine glands, concentrated in the axillae and areolar regions. The secretions from these glands could be easily broken down by bacteria to produce odors. Based on secretory activity and moisture accumulation, the body can be functionally partitioned into three distinct areas: axillae, anterior chest, and dorsal torso as high humidity areas, posterior torso, lateral lumbar regions, and upper arms as moderate humidity areas, and shoulders, forearms, and remaining anatomical areas as low humidity areas.

In addition to investigating the distribution of heat and humidity of the human body during exercise, the deodorization, thermal insulation, and mechanical durability of functional clothing were also divided into different regions. For odor resistance, the armpit was the area with the highest odor intensity, the chest and back, which had the highest sweat output, were areas with medium odor intensity, and the remaining areas were those with low odor intensity. For thermal insulation performance, the abdomen was the area with the highest level of thermoregulatory insulation, the collar, shoulders, and sides of the waist were areas with a medium level of cold protection and warmth retention, and the chest, back, and arms were areas with a lower level of cold protection and warmth retention. Also, fabrics with better wear resistance should be located on the collar, cuffs, shoulders, armpits, and sides of the waist, while with excellent burst strength on the elbow joints.

In summary, the outdoor clothing was divided into eight functional areas, seen in Figure 5.

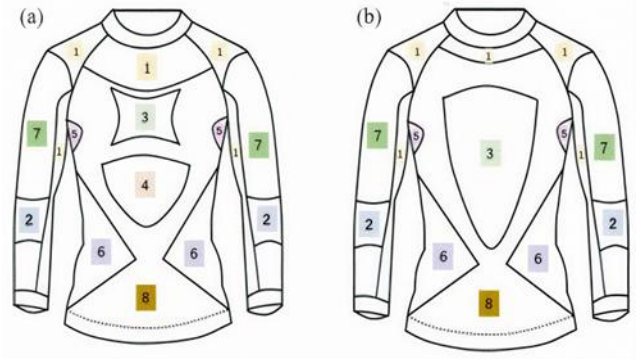

Figure 5. Partition diagram of outdoor function clothing, (a) Front side (b) Back side, Zone 1 for abrasion resistance and anti-pilling, Zone 2 for high elasticity and anti-burst, Zone 3 for air permeability and convection, Zone 4 for thermal insulation and cold protection, Zone 5 for deodorizing and moisture-wicking, Zone 6 for air permeability and moisture permeability, Zone 7 for high elasticity and moisture-wicking, and Zone 8 for moisture-wicking and deodorizing.

The Type II leaf-vein branch structure was employed in Zone 1 . The leaf vein branch structure of Type I was more suitable in Zone 2. The main vein structure was chosen in Zone 3 to accelerate gas flow and enhance breathability and moisture management

Textile Science & Research Journal
ISSN: 3059-846X Volume – 1, Issue – 1, 2025
DOI: https://doi.org/10.63456/tsrj-1-1-29

with air channels. The secondary leaf vein structure was selected in Zone 4, which had relatively high temperature that the body was prone to catching a chill during the cooling process after exercise. The armpit in Zone 5 had high perspiration accumulation, which was difficult to evaporate and had a strong odor. Therefore, deodorizing and moisture wicking fabrics of a leaf bubble structure implemented. The sweat secretion and heat generation in the side waist area of Zone 6 were low-activity, thus a leaf macropore structure with good breathability and moisture permeability was chosen. The leaf pinhole texture tissue with better resistance to bursting and moisture conductivity and sweat drainage performance was selected in Zone 7, which had many muscle groups, a large amount of sweat secretion, and a large range of motion. The main and secondary vein small grid structure with the best moisture and sweat drainage and wear resistance, and good odor resistance was in Zone 8.

KNITTING OF SEAMLESS GARMENT BASED ON ERGONOMICS

According to the style, size and structure of the wool seamless garments, the tissue diagrams (PAT) was inputted into the graphic design software (Photon), and the number of stitches based on the size of the functional garment was determined. Then, different structures with different colors according to the style was filled. The SDI diagrams were illustrated in Figures 6. The tissue diagrams (PAT) was filled into the SDI diagram to obtain the DIS diagram as shown in Figure 7. The generated DIS diagram was imported into the D3P software, with the yarn threading mode selected and the knitting cycle set, and then the on-machine file was generated in Figure 8.

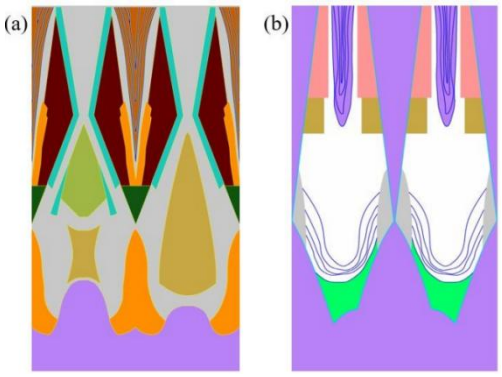

Figure 6. SDI diagram of bionic outdoor functional clothing, (a) body (b) sleeve

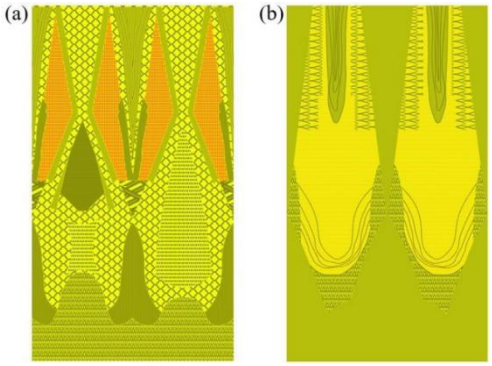

Figure 7. DIS diagram of bionic outdoor functional clothing, (a) body (b) sleeve

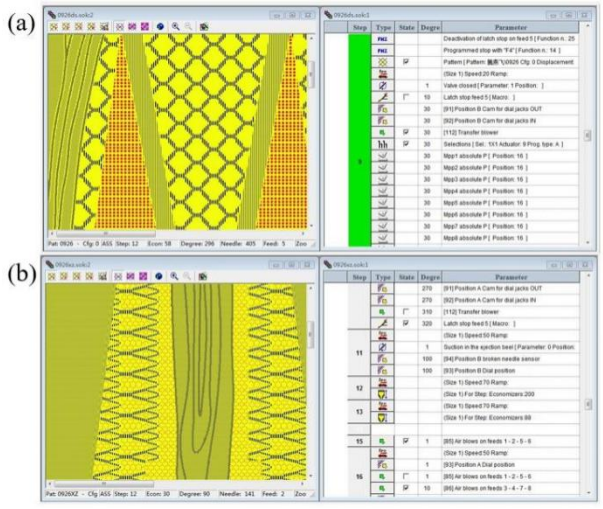

Figure 8. Knitting program of bionic outdoor functional clothing, (a) body (b) sleeve

Wool seamless clothing was knitted with 30-60r/min. Bionic wool seamless garment based ergonomics after finishing and setting shown in Figure 9.

Textile Science & Research Journal
ISSN: 3059-846X Volume – 1, Issue – 1, 2025
DOI: https://doi.org/10.63456/tsrj-1-1-29

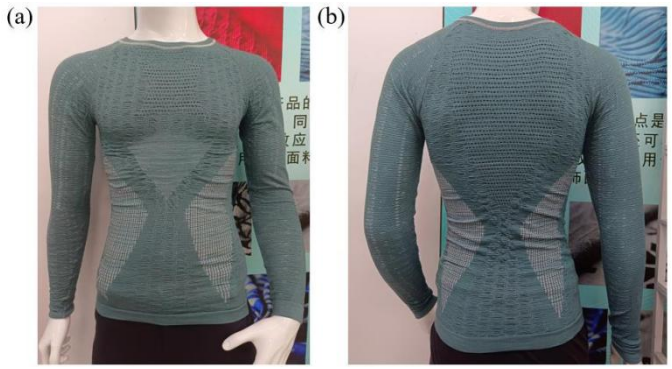

Figure 9. Photos of bionic wool seamless garment based ergonomics, (a) Right side (b) Reverse side

CHARACTERIZATIONS

WOOL FABRIC PROPERTIES
ODOR RESISTANCE

Based on GB/T 33610-2017 standard, a self-built detection system was used to measure the ammonia removal rate and acetic acid removal rate of bionic knitted fabric, as shown in Figure 10. Each sample had an area of 10×10 cm^2. Three tests were conducted for each test group, and the average value was adopted.

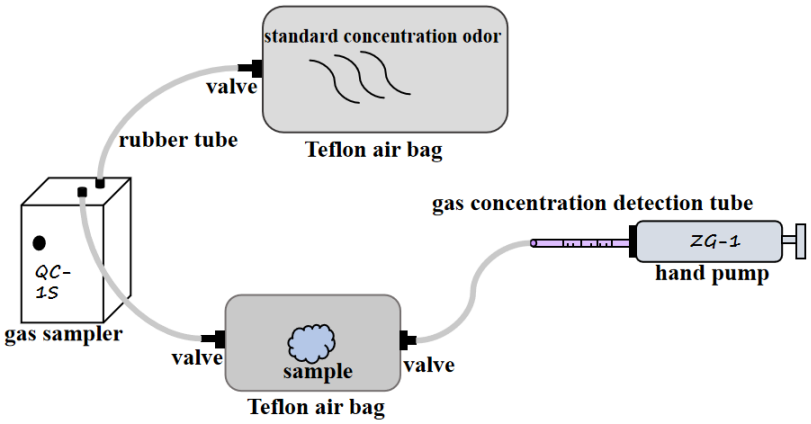

Figure 10. Deodorant rate detection device

THERMAL-MOISTURE COMFORT

YG606G thermal resistance & moisture resistance tester was evaluate the thermal resistance, heat transfer coefficient and Clo value according to ISO 11092-2014. Each sample had an area of 35×35cm2. Three tests were conducted for each fabric type, and thee average value is calculated.

YG461E-III air permeability tester was used to measure the air permeability of bionic knitted fabrics, each sample was tested 10 times and the average value was obtained according to ISO 9237-1995.

YG601H-II moisture permeability tester was measured fabric moisture permeability according to ASTM E96 cup method. The diameter of each circular sample was 70mm. The test was repeated 3 times and then averaged, the test was repeated three times and the average value was taken.

The moisture management tester was used to measure the cumulative unidirectional transfer index and evaluate overall moisture management performance of bionic knitted fabrics according to ASTM D1776-2008. Each fabric was tested five times, and the average value was adopted.

Textile Science & Research Journal
ISSN: 3059-846X Volume – 1, Issue – 1, 2025
DOI: https://doi.org/10.63456/tsrj-1-1-29

MECHANICAL PROPERTIES

According to ISO 12945-2: 2000 Textiles-Determination of Pilling and Balling Performance Part 2: Utilized modified Martindale Method, the YG401 abrasion tester was assessed the pilling and balling behavior of bionic knitted fabrics. Three circular samples with a diameter of 140 mm were cut from each fabric type, used the fabric itself as the abrasive material. Subjective evaluations were conducted at friction cycle counts of 125, 500, 1000, 2000, 5000, and 7000. Three observers rated the samples inside a rating box based on a five-grade scale, where 5 indicates the best and 1 the worst performance.

The HD026N electronic fabric strength tester was used to measure the bursting strength of bionic knitted fabrics based on ISO 13938-1: 1999. For each fabric type, five circular samples with a diameter of 50 mm were prepared. The test was conducted with a gauge length of 350 mm and a steel ball speed of 250 mm/min.

Based on ISO 13934-2: 1999 standard, the testing instrument was used to measure the warp and weft tensile breaking tenacity and elongation at break of fabrics. Each sample had dimensions of 200 mm×50 mm with a 100 mm gauge length, and stretching was performed at a constant speed of 100 mm/min.

All tests were conducted under controlled conditions where temperature was maintained at (20 ± 2)℃ and humidity was kept at 65% ± 2% for 24 hours of preconditioning. The final results were determined by calculating the average value.

THERMAL PROPERTIES AND SENSORY EVALUATION OF WOOL SEAMLESS GARMENTS

THERMAL PROPERTIES

The test personnel wore the outdoor functional clothing designed in this study and regular sportswear (raw material composition: 90% nylon / 7% polyester / 3% spandex) respectively. First, they remained still for 10 minutes in a perceived temperature of 21°C and a humidity of 45% of an outdoor environment to allow the functional clothing to reach a balance with the body. At this point, made the first measurement (FLIR-E6390, Estonia) using an infrared thermal imaging camera to observe the temperature distribution of the human body. After completed a 30-minute run at a constant speed of 16 km/h, recorded the changes in body temperature at 0 minutes, 3 minutes, 5 minutes, 7 minutes, and 15 minutes respectively.

SENSORY EVALUATION

A standardized sensory evaluation protocol was implemented to evaluate the odor resistance of the outdoor functional clothing during actual wear. Two days with the same meteorological conditions in autumn were selected which the daytime temperature ranged between 18°C and 22°C, the humidity was 38% ±5% and the testing period was set from 13:00 to 18:00 hours to conduct experiment. Three graduate students aged between 23 to 25 years wore the outdoor functional clothing designed in this study to engage in a mountain climbing activity (with an elevation of 330 meters) on the first day of the experiment. After the physical activity, the worn garments were air-dried and allowed to cool for 30 minutes to ensure the evaporation of perspiration. Then three trained evaluators conducted sensory evaluations on the axillary and pectoral regions areas of the functional clothing. The odor concentration level of the clothing was assessed in compliance with the GB/T 33610-2019 standard, with each measurement performed in triplicate and the mean value of the results calculated. In order to make the experiment comparable, on the second day, the participants wore regular sportswear and followed the same route in the same time period to climb the mountain again, the underwent sensory evaluation.

RESULTS AND DISCUSSION

WOOL FABRIC PROPERTIES
ODOR RESISTANCE

The ammonia removal rate (ADR) and acetic acid removal rate (AADR) of bionic knitted fabrics were summarized in Table 2. Among eight bionic knitted fabric samples, the maximum ADR reached 99.50% while the minimum was 85.11%. For AADR, the highest value was 94.55% and the lowest was not less than 80.36%, with all samples exceeding the 80% threshold, demonstrating excellent deodorization capability. When compared with jersey fabrics, sample #7 demonstrated significantly superior odor resistance.

Textile Science & Research Journal
ISSN: 3059-846X Volume – 1, Issue – 1, 2025
DOI: https://doi.org/10.63456/tsrj-1-1-29

The variation in odor resistance among the eight fabric samples may be related to their fabric areal density. The three yarn types composing the fabrics were deodorant spandex, polypropylene, and wool. Among these, the yarns demonstrating significant odor-molecule removal were deodorant spandex and wool. Consequently, the odor resistance of the fabrics was closely correlated with the content of deodorant spandex and wool: The higher the content of deodorant spandex and wool, the greater the fabric weight became, thereby enhancing the odor resistance.

Table 2. Odor elimination property of bionic knitted fabrics

Sample NO.	ammonia				acetic acid			
	Initial concentration ppm	The concentration after 2 hours		ADR/%	Initial concentration ppm	The concentration after 2 hours		AADR /%
		Sample A	Blank B			Sample A	Blank B	
1#	100.00	5.50(0.60)	98.00	94.39%	30.00	3.00(0.40)	28.50	89.47%
2#	100.00	7.50(0.66)	98.00	92.35%	30.00	4.00(0.49)	29.00	86.21%
3#	100.00	5.00(0.45)	94.00	94.68%	30.00	2.50(0.33)	28.50	91.23%
4#	100.00	13.50(1.91)	96.00	85.94%	30.00	5.00(0.53)	27.00	81.48%
5#	100.00	11.00(1.22)	94.00	88.30%	30.00	4.50(0.39)	27.50	83.64%
6#	100.00	14.00(1.50)	94.00	85.11%	30.00	5.50(0.68)	28.00	80.36%
7#	100.00	0.50(0.03)	92.00	99.50%	30.00	1.50(0.11)	27.50	94.55%
8#	100.00	6.50(0.70)	95.00	93.16%	30.00	3.50(0.37)	28.50	87.72%
0#	100.00	4.50(0.55)	72.00	93.75%	30.00	2.00(0.31)	28.00	92.86%

THERMAL-MOISTURE COMFORT

According to Table 3, except for Sample #4, all other bionic knitted fabrics demonstrated significantly superior thermal insulation performance compared with conventional weft-flat knitted fabrics. Overall, bionic leaf-vein structured fabrics (Samples 2#, 1#, 3#, 8#, and 5#) exhibited better thermal insulation performance than bionic pore-structured fabrics (Samples 6# and 4#). This was because bionic leaf-vein fabrics feature a higher number of floating thread loops, greater fabric contraction, more air channels with tight spacing to trap a large amount of static air. In contrast, bionic pore-structured fabrics had a smooth surface that lacks air storage capacity. The excellent thermal insulation performance of Sample #7 was attributed to its large-area bubble-like protrusions, which effectively decelerated the airflow velocity between the fabric and skin.

The broad, uniformly distributed air channels of Sample #1 created extensive and numerous edge pores, thereby exhibiting the best air permeability. Conversely, Sample #8 demonstrated the poorest air permeability. This may be caused by the structural tightening effect from increased longitudinal contraction to restrict airflow and reduce permeability.

With the exception of Samples 4#, 5#, and 7#, the remaining bionic structured fabrics demonstrated significantly superior moisture permeability compared with conventional weft-flat knitted fabrics.

In accordance with the performance classification criteria and evaluation specifications of ASTM D1776-2008, all eight bionic knitted fabrics demonstrated unidirectional transport indices exceeding 300, fulfilling the requirements for excellent moisture absorption and wicking properties. Sample #3 and #7 demonstrated significantly superior moisture management performance relative to conventional weft-flat knitted fabrics.

Textile Science & Research Journal
ISSN: 3059-846X Volume – 1, Issue – 1, 2025
DOI: https://doi.org/10.63456/tsrj-1-1-29

Table 3. Thermal-moisture comfort of bionic knitted fabrics

Sample NO.	Thermal resistance ($m^2 \times K \times W^{-1}$)	Heat transfer coefficient ($W \times (m^2 \times °C)^{-1}$)	Clo value (10^{-3}clo)	Air permeability (mm/s)	Moisture permeability ($g/(m^2 \cdot h)$)	Unidirectional transfer index
1#	74.100(8.65)	13.55	478.0	390.78(35.75)	454.77(58.29)	324.210(26.49)
2#	112.233(15.38)	9.07	723.7	226.78(28.64)	237.81(32.47)	369.700(36.17)
3#	71.675(9.84)	14.00	462.3	280.36(32.44)	292.23(38.51)	409.610(48.28)
4#	42.633(6.30)	24.29	275.0	181.04(19.85)	154.77(25.38)	381.250(28.46)
5#	51.733(6.89)	19.41	333.7	302.44(36.27)	112.90(13.57)	377.620(42.68)
6#	44.950(7.06)	22.34	289.6	352.78(43.84)	259.36(31.46)	385.240(33.12)
7#	95.967(10.46)	10.67	618.7	331.56(29.95)	180.04(19.31)	405.930(56.40)
8#	53.475(7.82)	18.68	344.8	173.32(21.56)	225.80(27.93)	365.710(32.57)
0#	43.200(5.35)	23.27	263.0	49.00(8.96)	189.00(18.74)	402.550(46.81)

MECHANICAL PROPERTIES

The results of multiple abrasion tests on knitted fabrics were presented in Table 4, the physical appearance of eight fabric samples after 7,000 friction cycles were showed in Figure 11. The fabrics were revealed three distinct performance gradients, Gradient 1 included Samples 1#, 2#, 3#, 7#, and 8#, which maintained clear and regular texture patterns after 7,000 cycles, demonstrating the best abrasion resistance. Gradient 2 consisted of Sample 5#, showing minor fuzz formation but still exhibiting satisfactory. Gradient 3 comprised Samples 4# and 6#, which exhibited slight fuzzing and moderate. The variation among the eight bionic fabrics may primarily relate to their surface structure: Fabrics with more floating thread loops exhibit tighter surface contraction, thereby enhancing their wear resistance.

Table 4. The pilling results of bionic knitted fabrics after repeated rubbing

Sample NO.	Number of Frictions					
	125	500	1000	2000	5000	7000
1#	5.0	5.0	5.0	5.0	5.0	5.0
2#	5.0	5.0	5.0	5.0	5.0	5.0
3#	5.0	5.0	5.0	5.0	5.0	5.0
4#	5.0	5.0	5.0	5.0	4.5	4.0
5#	5.0	5.0	5.0	5.0	5.0	4.5
6#	5.0	5.0	5.0	5.0	4.5	4.0
7#	5.0	5.0	5.0	5.0	5.0	5.0
8#	5.0	5.0	5.0	5.0	5.0	5.0

Textile Science & Research Journal
ISSN: 3059-846X Volume – 1, Issue – 1, 2025
DOI: https://doi.org/10.63456/tsrj-1-1-29

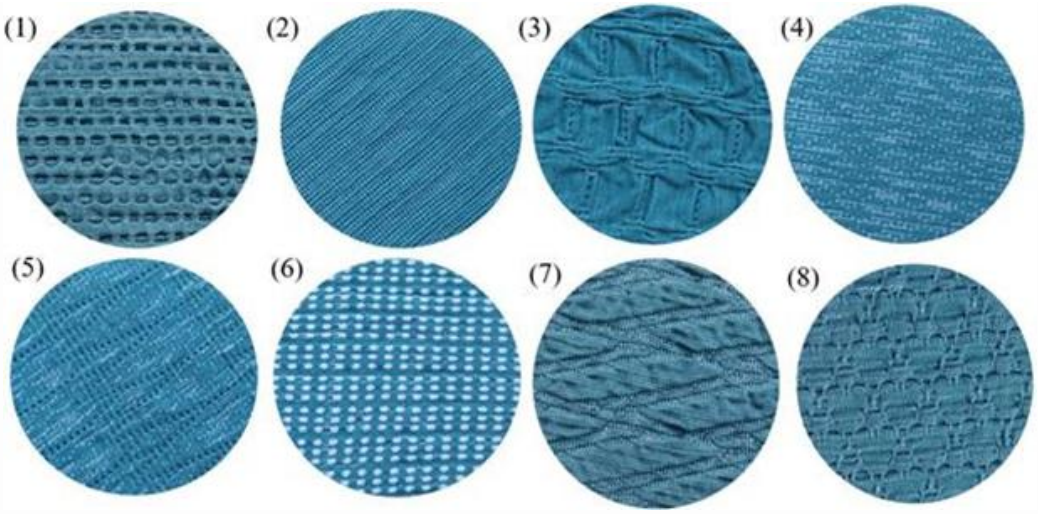

Figure 11. Physical images of eight fabrics after 7000 frictions

Bursting strength was an important indicator reflecting the degree of deformation and rupture in fabrics under external compressive forces. According to Table 5, the eight bionic fabrics were ranked from highest to lowest bursting strength as follows: Samples 5#, 4#, 2#, 1#, 8#, 3#, 6#, and 7#. The burst height of fabrics correlates with their elasticity, with rankings from highest to lowest as: Samples 5#, 1#, 7#, 3#, 6#, 4#, 8#, and 2#. Notably, Sample 5# exhibited superior bursting performance in both categories.

Table 5. Bursting performance of bionic knitted fabrics

Sample NO.	Bursting strength N	Bursting Height mm	Bursting work J
1#	404.50(37.92)	58.41(8.48)	1.27(0.11)
2#	427.85(48,25)	32.54(2.71)	0.68(0.05)
3#	359.65(35.83)	51.90(6.90)	1.10(0.09)
4#	494.30(58.27)	47.44(5.27)	1.01(0.09)
5#	510.20(63.42)	62.30(8,37)	1.27(0.15)
6#	353.05(33.18)	48.00(3.56)	0.85(0.07)
7#	317.40(25.83)	56.16(7.84)	0.92(0.10)
8#	377.35(30.56)	46.13(3.49)	0.89(0.06)

During sports activities, functional garments were required to possess excellent tensile strength and tear resistance to withstand external forces such as stretching and pulling. As shown in Table 6, the eight bionic knitted fabrics demonstrated greater warp breaking strength and elongation at break compared to the weft direction. This phenomenon occurred primarily due to the higher density of warp floating loops in the fabrics, the jacquard loops primarily bore the mechanical load when the fabric was stretched. Conversely, during weft stretching, all loop structures experienced uniformly subjected to force. A horizontal comparison of the eight fabrics revealed that Sample #2 demonstrated the highest breaking strength, which correlated with its maximum fabric density and the largest number of load-bearing loops. Meanwhile, Sample #8 exhibited the highest elongation at break, indicating superior softness and elasticity inherent in its structure.

Textile Science & Research Journal
ISSN: 3059-846X Volume – 1, Issue – 1, 2025
DOI: https://doi.org/10.63456/tsrj-1-1-29

Table 6. Breaking force of bionic knitted fabrics

Sample NO.	Warp direction J /Weft direction W	Breaking strength N	Breaking tenacity N/mm	Elongation at break %
1#	J	41.65(6.39)	0.83(0.09)	200.55(18.48)
	W	97.61(11.44)	1.95(0.26)	241.34(27.94)
2#	J	58.39(5.92)	1.17(0.13)	97.80(8.47)
	W	113.34(16.48)	2.27(0.29)	203.26(21.10)
3#	J	44.04(5.00)	0.88(0.07)	171.45(15.33)
	W	82.25(10.29)	1.65(0.19)	256.26(20.36)
4#	J	45.15(5.84)	0.90(0.10)	146.25(15.45)
	W	55.54(8.11)	1.11(0.14)	265.69(28.37)
5#	J	35.06(3.01)	0.70(0.05)	158.84(13.18)
	W	55.13(6,83)	1.10(0.12)	274.59(32.80)
6#	J	39.77(4.19)	0.80(0.06)	152.60(16.84)
	W	43.08(4.90)	0.87(0.08)	225.08(25.29)
7#	J	33.24(3.04)	0.67(0.04)	137.00(10.30)
	W	101.89(13.93)	2.04(0.27)	248.13(22.31)
8#	J	44.86(3.97)	0.90(0.11)	238.63(24.47)
	W	101.34(8.39)	2.03(0.28)	280.42(31.34)

GREY NEAR-OPTIMAL EVALUATION

GREY NEAR-OPTIMAL MODELS

the diversity of performance indicators and varying units of bionic knitted fabrics that a single metric could not comprehensively evaluate their overall performance, the grey near-optimal method was employed to synthesize multiple performance parameters for holistic assessment.[23] The comprehensive evaluation process of grey near-optimal models typically comprised the following four critical steps.

Step 1: Based on the test results of thr samples and their performance, the grey matrix $R_{n\times m}$ was constructed.

$$R_{n\times m} = \begin{bmatrix} C_1 \\ \vdots \\ C_2 \end{bmatrix} \begin{bmatrix} R_{11} & \cdots & R_{1m} \\ \vdots & R_{ij} & \vdots \\ R_{n1} & \cdots & R_{nm} \end{bmatrix} \quad (1)$$

In the formula, C_i was the i-th performance indicator;R_{ij} was the Grey element value of Sample j for the i-th performance.

Step 2: Actual datas were substitute into Equation (1), and the grey element values R_{ij} was converted into white-gray element values X_{ij}, see Equation 2.

$$X_{n\times m} = \begin{bmatrix} C_1 \\ \vdots \\ C_n \end{bmatrix} \begin{bmatrix} X_{11} & \cdots & X_{1m} \\ \vdots & X_{ij} & \vdots \\ X_{n1} & \cdots & X_{nm} \end{bmatrix} \quad (2)$$

In the formula, X_{ij} was White-gray element value of Sample j for the ith indicator.

Textile Science & Research Journal
ISSN: 3059-846X Volume – 1, Issue – 1, 2025
DOI: https://doi.org/10.63456/tsrj-1-1-29

Step 3: Due to the diverse units and meanings of performance indicators, a unified normalization process was required to quantitatively compare the overall performance differences among bionic knitted fabrics. This was achieved by mapping each white-gray element value X_{ij} to a corresponding effectiveness measure F_{ij}, thereby constructing the near-optimal white-gray matrix $F_{n\times m}$. Depending on whether the indicator was "higher-is-better," "moderate-is-better," or "lower-is-better": Apply upper/lower limit effectiveness measures as specified in Equations (3)~(5).

Higher-Is-Better Indicator:

$$F_{ij} = \frac{x_{ij}}{max(x_{ij},\ u_{max})} \tag{3}$$

Moderate-Is-Better Indicator:

$$F_{ij} = \frac{max(x_{ij},\ u_0)}{max(x_{ij},\ u_{max})} \tag{4}$$

Lower-Is-Better Indicator:

$$F_{ij} = \frac{min(x_{ij},\ u_{min})}{x_{ij}} \tag{5}$$

In the formula, u_{max} was the maximum value of X_{ij} in row i, u_0 was the optimal value, and u_{min} was the minimum value.

Step 4: According to equation (6), the effectiveness measure F_{ij} was substituted into the model to construct the white element row matrix F_s. Then, the gray near-optimality degree of each fabric was calculated through this procedure.

$$F_s = S_j[S_1\ S_2 \cdots S_m] = S_j\left[\frac{1}{n}\sum_{i=1}^{n} F_{i1},\ \frac{1}{n}\sum_{i=1}^{n} F_{i2},\ \cdots,\ \frac{1}{n}\sum_{i=1}^{n} F_{im}\right] \tag{6}$$

In the formula: S_j was defined as the gray near-optimality degree of sample j. A higher value of S_j indicates better comprehensive performance of the fabric.

GREY COMPREHENSIVE EVALUATION

Following the established steps to constructed the grey near-optimal model and substituted the test results of eight bionic knitted fabrics into Equations (1)~(5). After obtained the effectiveness measures F_{ij}, the near-optimal white-gray matrix $F_{8\times8}$ was established. The performance indicators were defined as follows: C_1 represented the ammonia removal rate (ADR), C_2 denoted the thermal resistance value, C_3 corresponded to air permeability, C_4 was moisture permeability, C_5 was the cumulative unidirectional transfer index (OTWC), C_6 indicated the abrasion level, C_7 refered to bursting strength, and C_8 was the warp breaking elongation rate. Finally, the effectiveness measures F_{ij} was substituted into Equation (6) to calculate the comprehensive near-optimal degree F_S of each fabric.

First, the gray matrix (7) was established.

$$R_{8\times8} = \begin{bmatrix} C_1 \\ C_2 \\ C_3 \\ C_4 \\ C_5 \\ C_6 \\ C_7 \\ C_8 \end{bmatrix} \begin{bmatrix} R_{11} & R_{12} & R_{13} & R_{14} & R_{15} & R_{16} & R_{17} & R_{18} \\ R_{21} & R_{22} & R_{23} & R_{24} & R_{25} & R_{26} & R_{27} & R_{28} \\ R_{31} & R_{32} & R_{33} & R_{34} & R_{35} & R_{36} & R_{37} & R_{38} \\ R_{41} & R_{42} & R_{43} & R_{44} & R_{45} & R_{46} & R_{47} & R_{48} \\ R_{51} & R_{52} & R_{53} & R_{54} & R_{55} & R_{56} & R_{57} & R_{58} \\ R_{61} & R_{62} & R_{63} & R_{64} & R_{65} & R_{66} & R_{67} & R_{68} \\ R_{71} & R_{72} & R_{73} & R_{74} & R_{75} & R_{76} & R_{77} & R_{78} \\ R_{81} & R_{82} & R_{83} & R_{84} & R_{85} & R_{86} & R_{87} & R_{88} \end{bmatrix} \tag{7}$$

Subsequently, actual data was substituted to construct the whitened grey element matrix (8).

Textile Science & Research Journal
ISSN: 3059-846X Volume – 1, Issue – 1, 2025
DOI: https://doi.org/10.63456/tsrj-1-1-29

$$R_{8\times8}=\begin{bmatrix}C_1\\C_2\\C_3\\C_4\\C_5\\C_6\\C_7\\C_8\end{bmatrix}\begin{bmatrix}94.39 & 92.35 & 94.68 & 85.94 & 88.30 & 85.11 & 99.50 & 93.16\\ 74.10 & 112.2 & 71.68 & 42.63 & 51.73 & 44.95 & 95.97 & 53.48\\ 390.7 & 226.7 & 280.2 & 181.0 & 302.4 & 352.7 & 331.5 & 173.3\\ 454.7 & 237.8 & 292.2 & 154.7 & 112.9 & 259.3 & 180.0 & 225.8\\ 324.2 & 369.7 & 409.6 & 381.2 & 377.6 & 385.2 & 405.9 & 365.7\\ 5.00 & 5.00 & 5.00 & 4.00 & 4.50 & 4.00 & 5.00 & 5.00\\ 404.5 & 427.8 & 359.6 & 494.3 & 510.2 & 353.0 & 317.4 & 377.3\\ 200.5 & 97.80 & 171.4 & 146.25 & 158.8 & 152.6 & 137.0 & 238.6\end{bmatrix} \quad (8)$$

The values were then mapped to the interval [0,1], resulting in the matrix $F_{n\times m}$ (9).

$$R_{8\times8}=\begin{bmatrix}C_1\\C_2\\C_3\\C_4\\C_5\\C_6\\C_7\\C_8\end{bmatrix}\begin{bmatrix}0.95 & 0.93 & 0.95 & 0.86 & 0.89 & 0.86 & 1.00 & 0.94\\ 0.66 & 1.00 & 0.64 & 0.38 & 0.46 & 0.40 & 0.86 & 0.48\\ 1.00 & 0.58 & 0.72 & 0.46 & 0.77 & 0.90 & 0.85 & 0.44\\ 1.00 & 0.52 & 0.64 & 0.34 & 0.25 & 0.57 & 0.40 & 0.50\\ 0.79 & 0.90 & 1.00 & 0.93 & 0.92 & 0.94 & 0.99 & 0.89\\ 1.00 & 1.00 & 1.00 & 0.80 & 0.90 & 0.80 & 1.00 & 1.00\\ 0.79 & 0.84 & 0.70 & 0.97 & 1.00 & 0.69 & 0.62 & 0.74\\ 0.84 & 0.41 & 0.72 & 0.61 & 0.67 & 0.64 & 0.57 & 1.00\end{bmatrix} \quad (9)$$

Finally, the row matrix was calculated to obtain the fabric's comprehensive near-optimality degree F_s (10).

$$F_s = S_j[S_1 \cdots S_8] = [0.879\ \ 0.773\ \ 0.796\ \ 0.669\ \ 0.733\ \ 0.725\ \ 0.786\ \ 0.749] \quad (10)$$

In the formula: S_j is defined as the gray near-optimality degree of fabric j.

The gray near-optimal degree scores of eight bionic knitted fabrics was revealed after analysis of the near-optimal white-gray element matrix within the grey near-optimal model. These scores directly reflected the comprehensive performance superiority of the fabrics, with the ranking from highest to lowest as follows: 1#, 3#, 7#, 2#, 8#, 5#, 6#, and 4#. Notably, Sample 1# achieved the highest gray near-optimal degree, indicating its outstanding comprehensive performance across all tested metrics.

GREY RELATIONAL ANALYSIS

Grey relational analysis was applied to calculate the correlation degree between performance indicators and the grey near-optimality degree, and the specific weights of fabric test indicators influencing the grey near-optimality degree were analyzed in depth. The near-optimality degrees of fabric samples 1#-8# (0.879, 0.773, 0.796, 0.669, 0.733, 0.725, 0.786, 0.749) were defined as the reference sequence L_0, while the comparative sequence L_i was set as the test result of the i-th indicator for fabric m. The test indicators included ammonia elimination rate, thermal resistance value, air permeability, moisture permeability, unidirectional transfer index, friction grade, bursting strength, and warp breaking elongation. The correlation degree r_i for each performance was calculated through the following procedure:

Step 1: The dimensionless mean normalization was performed according to equation (11).

$$l_{ij} = \frac{L_{ij}}{L_i} \quad (11)$$

In the formula: I_{ij} was defined as the dimensionless mean value of the i -th performance for fabric j; L_{ij} represented the original test data of the j-th performance for fabric j; L_1 was the mean value of the test data for the i-th fabric row.

Step 2: The difference sequence was calculated according to equation (12).

$$V_{ij} = |l_{ij} - l_j| \quad (12)$$

In the formula: V_{ij} was defined as the absolute difference between the reference and comparative sequences for the i-th performance of fabric j; I_j represented the grey near-optimality degree of fabric j within I_0. Step 3: The correlation coefficient between the reference and comparative sequences was calculated according to equation (13).

Textile Science & Research Journal
ISSN: 3059-846X Volume – 1, Issue – 1, 2025
DOI: https://doi.org/10.63456/tsrj-1-1-29

$$H_{ij} = \frac{W_{min} + pW_{max}}{V_{ij} + pW_{max}} \quad (13)$$

In the formula: H_{ij} was defined as the correlation coefficient between the reference sequence and the i-th row comparative sequence; W_{min} denoted the minimum value of the difference sequence, and W_{max} denoted the maximum value of the difference sequence; p was the discrimination coefficient with a fixed value of 0.5.

Step 4: The correlation degree between the reference and comparative sequences was calculated according to equation (14).

$$r_i = \frac{1}{m}\sum_{j=1}^{m} H_{ij} \quad (14)$$

In the formula: r_i was defined as the correlation degree between the reference and comparative sequences; a higher value indicates a stronger correlation.

The correlation coefficients between each performance indicator and the near-optimality degree were calculated and ranked, ranked in descending order as follows: friction grade (0.827), bursting strength (0.811), unidirectional transport index (0.774), warp breaking elongation (0.767), ammonia elimination rate (0.721), thermal resistance (0.717), air permeability (0.699), and moisture permeability (0.683). Among these, friction grade and bursting strength exhibit the strongest correlation on the comprehensive performance of the bionic knitted fabric, while moisture permeability had the weakest association. In summary, the performance indicators and comprehensive performance rankings of the eight bionic knitted fabrics were listed in Table 7, providing a reference basis for the zonal design of outdoor functional clothing.

Table 7. Comprehensive sorting of bionic knitted fabrics performance index

Performance	Comprehensive sorting
Odor resistance	$7^{\#}>1^{\#}=3^{\#}>8^{\#}>2^{\#}>5^{\#}>4^{\#}=6^{\#}$
Thermal-moisture comfort	$2^{\#}>7^{\#}>1^{\#}>3^{\#}>8^{\#}>5^{\#}>6^{\#}>4^{\#}$
Air permeability	$1^{\#}>6^{\#}>7^{\#}>5^{\#}>3^{\#}>2^{\#}>4^{\#}>8^{\#}$
Moisture permeability	$1^{\#}>3^{\#}>6^{\#}>2^{\#}>8^{\#}>7^{\#}>4^{\#}>5^{\#}$
Unidirectional moisture transfer performance	$3^{\#}>7^{\#}>6^{\#}>4^{\#}>5^{\#}>2^{\#}>8^{\#}>1^{\#}$
Wear resistance	$1^{\#}=2^{\#}=3^{\#}=7^{\#}=8^{\#}>5^{\#}>4^{\#}=6^{\#}$
Bursting performance	$5^{\#}>4^{\#}>2^{\#}>1^{\#}>8^{\#}>3^{\#}>6^{\#}>7^{\#}$
Tensile fracture performance	$8^{\#}>1^{\#}>3^{\#}>5^{\#}>6^{\#}>4^{\#}>7^{\#}>2^{\#}$
Comprehensive performance	$1^{\#}>3^{\#}>7^{\#}>2^{\#}>8^{\#}>5^{\#}>6^{\#}>4^{\#}$

THERMAL PROPERTIES AND SENSORY EVALUATION OF WOOL SEAMLESS GARMENTS

THERMAL PROPERTIES

The results of the temperature measurement by infrared thermal imaging were illustrated in Figure 12. The surface temperature around the chest area of both garments was approximately 29.8°C before running. But after exercise, the surface temperature of the regular sportswear was 32.4°C, while that of the functional clothing was 32.6°C. During the first 3 minutes of rest following exercise cessation, heart rate remained elevated and the body continued to generate heat. At the 3th minute mark, the temperature of the regular sportswear reached as high as 34.2°C, which was 1.4°C higher than that of the functional clothing. Subsequently, the evaporation of sweat caused the body to start cooling down. At the 15th minute mark, the temperature of regular sportswear was 28.8°C, 1°C lower than before running; while that of the functional garment was 30.2°C, only 0.3°C different from before running. During the entire test, the maximum temperature difference of regular sportswear was 4.4°C, while for functional clothing it was only 2.9°C. Therefore, the outdoor functional clothing had excellent thermal-moisture comfort that was better at maintaining a stable body temperature during exercise to prevent the body from feeling excessively hot or cold.

Textile Science & Research Journal
ISSN: 3059-846X Volume – 1, Issue – 1, 2025
DOI: https://doi.org/10.63456/tsrj-1-1-29

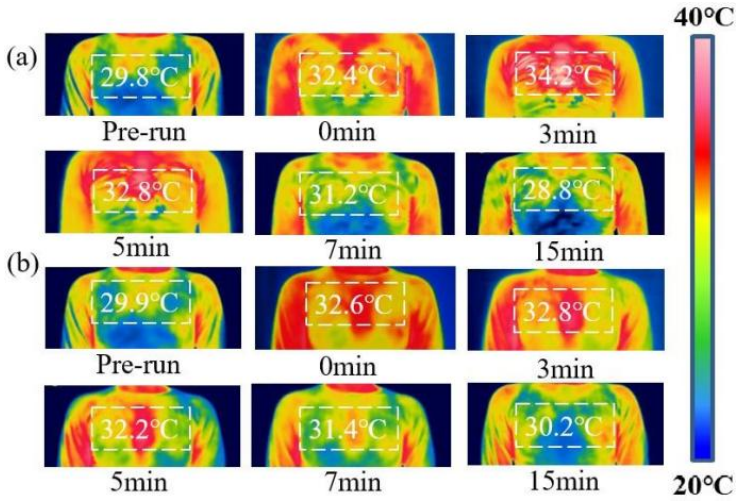

Figure 12. Infrared images, (a) Ordinary sportswear (b) Outdoor functional clothing in this work

SENSORY EVALUATION

Table 8 showed the results of the sensory evaluation tests. The odor intensity was divided into the following six levels: 0 - No odor; 1 - Slight odor, unable to identify the type of odor; 2 - Mild odor, able to identify the type of odor; 3 - Moderate odor, easily noticeable; 4 - Strong odor; 5 - Very strong odor. Overall, the outdoor functional clothing had a lower odor level compared to regular sportswear. Especially in areas with stronger odors such as the underarms, the functional clothing also demonstrated effective odor elimination.

Table 8. The intensity of odors in various parts of sportswear

participant	Odor intensity level of functional clothing (Underarm)	odor intensity level of regular sportswear (Underarm)	Odor intensity level of functional clothing (Chest)	odor intensity level of regular sportswear (Chest)
A	0.5	4.5	0	2.5
B	0.0	3.0	0	3.5
C	1.0	5.0	0	2.0

CONCLUSION

In this work, eight bionic knitted fabrics inspired by Victoria amazonica were deveioped using wool and a deodorizing spandex/polypropylene covered yarn. After analyzing odor resistance and thermal-moisture comfort, we found that, compared with the a plain weft-knitted structure, most bionic fabrics showed improved performance and met the mechanical requirements of outdoor functional clothing. A Grey Near-Optimal Model was developed to comprehensively evaluate the biomimetic textiles. The results showed that the main vein structure had the best comprehensive performance, with an air permeability of 390.78 mm/s and a moisture permeability of 454.77 g/(m2×h).

The outdoor functional clothing was partitioned into eight zones based on the body's heat, humidity, and odor distributions. To evaluate and thermal-moisture comfort, a commercial sportswear garment composed of polyester/spandex covered yarn and nylon was used for comparison. An infrared thermal imaging camera was used to measure body temperature changes before and after exercise, and trained panelists conducted sensory odor evaluations.The results showed the maximum temperature difference between the start of exercise and the third minute after exercise of the wool seamless garments for outdoor sports was 2.9°C, which is lower than the 4.4°C difference observed in regular sportswear, and the odor intensity was rated as slight. This verifies the excellent deodorizing performance and thermal-moisture comfort of this clothing.

ACKNOWLEDGMENT

This work was supported by the Jiangsu Province Technology Project "Biodegradable temperature-sensitive intelligent polyurethane filament with application development" (Project number: BE2022131).

REFERENCES

1. Lee S Y, Kim J H, Lee J S. Needs and sensibility of functional fabrics for outdoor sportswear[J]. Textile Science and Engineering, 2010, 47(3): 163-172.
2. Li HY, Mo Y, Dong GL, et al. Development of Partition-Designed Outdoor Workwear with Optimal Fabric Selection[J]. AATCC Journal of Research,2024,Vol.11(4): 300-315.
3. Dong ZJ, Ding YQ, Han LY, et al. Heat and sweat regulating performance of zoning structure weft-knitted sportswear[J]. Textile Research Journal, 2024: 00405175241268521.
4. Varadaraju R, Srinivasan J. Design of sports clothing for hot environments[J]. Applied ergonomics, 2019, 80: 248-255.
5. Ke Y, Zheng Q. Development of mining workwear with high ergonomic performance fabrics based on the modular design concept[J]. International Journal of Occupational Safety and Ergonomics, 2023, 29(2): 547-554.
6. Li HY, Mo Y, Dong GL, et al. Development of partition-designed outdoor workwear with optimal fabric selection[J]. AATCC Journal of Research, 2024, 11(4): 300-315.
7. Xue ZB, Jin P, Jiang RT. Design and evaluation of a novel interactive firefighter clothing with multiple functionalities[J]. Textile Research Journal, 2023, 93(1-2): 221-241.
8. Chen HY, Lin BS, Yang SR, et al. Design of Automatic Adjustment Non-Contact Sensing Smart Clothing[J]. IEEE Sensors Journal, 2024.
9. Granberry R, Eschen K, Holschuh B, et al. Functionally graded knitted actuators with NiTi-based Shape Memory Alloys for topographically self-fitting wearables[J]. Advanced materials technologies, 2019, 4(11): 1900548.
10. Wang F, Guo WL, Tian Y, et al. Thermal comfort of medical protective clothing under high temperature and high humidity[J]. Building and Environment, 2025, 270: 112570.
11. Lapkovska E, Daboliņa I, Siliņa L, et al. Development of an ergonomic protective suit for physiotherapists during the COVID-19[J]. Journal of Engineered Fibers and Fabrics, 2022, 17: 15589250221091819.
12. Kim HA. Water repellency/proof/vapor permeability characteristics of coated and laminated breathable fabrics for outdoor clothing[J]. Coatings, 2021, 12(1): 12.
13. Knížek R, Tunák M, Tunáková V, et al. Effect of membrane morphology on the thermo-physiological comfort of outdoor clothing[J]. Journal of Engineered Fibers and Fabrics, 2024, 19: 15589250241265334.
14. Thangamuthu S, Pandurangan S. Investigation of moisture transfer properties of double-face weft knitted fabrics for sports clothing[J]. Journal of Industrial Textiles, 2022, 51(3_suppl): 5286S-5303S.
15. Zhu H, Gou ZG, Liu WM, et al. Biomimetic water-collecting materials inspired by nature[J]. Chemical Communications,2016,Vol.52(20): 3863-3879.
16. Graybill MT, Xu NW. Experimental studies of bioinspired shark denticles for drag reduction[J]. Integrative and Comparative Biology, 2024, 64(3): 742-752.
17. Parker AR, Lawrence CR. Water capture by a desert beetle [J]. Nature, 2001, 414(6859): 33-34.
18. Bixler GD, Bhushan B. Shark skin inspired low-drag microstructured surfaces in closed channel flow[J]. Journal of colloid and interface science, 2013, 393: 384-396.
19. Leon DA, Advincula RC. Reversible superhydrophilicity and superhydrophobicity on a lotus-leaf pattern[J]. ACS applied materials & interfaces, 2014, 6(24): 22666-22672.
20. Sasaki K, Tenjimbayashi M, Manabe K, et al. Asymmetric superhydrophobic/superhydrophilic cotton fabrics designed by spraying polymer and nanoparticles [J]. ACS applied materials & interfaces, 2016, 8(1): 651-659.
21. Chen YM, Li SJ, Li XL, et al. Liquid transport and real-time dye purification via lotus petiole-inspired long-range-ordered anisotropic cellulose nanofibril aerogels[J]. ACS Nano, 2021, 15(12): 20666-20677.
22. Box F, Erlich A, Guan JH, et al. Gigantic floating leaves occupy a large surface area at an economical material cost[J]. Science Advances, 2022, 8(6): 3790.
23. Liu SF, Yang YJ. Advances in Grey System Research (2004-2014) [J]. Journal of Nanjing University of Aeronautics &Aeronautics, 2015, 47(1): 1-18.